# Pressure-induced transformations in amorphous Si-Ge alloy

F. Coppari,[1,*] A. Polian,[1] N. Menguy,[1] A. Trapananti,[2] A. Congeduti,[3] M. Newville,[4] V. B. Prakapenka,[4] Y. Choi,[4] E. Principi,[5,6] and A. Di Cicco[1,5]

[1]*IMPMC-CNRS UMR 7590, Université P.et M. Curie, 4 pl. Jussieu, FR-75005 Paris, France*

[2]*CNR, Istituto Officina dei Materiali - OGG Grenoble c/o ESRF BP 220, 6 Rue Jules Horowitz FR-38043 Grenoble Cedex, France*

[3]*Synchrotron Soleil, L'Orme des Merisiers, St. Aubin FR-91192 Gif s/Yvette, France*

[4]*Center for Advanced Radiation Sources, University of Chicago, Chicago, Illinois 60637, USA*

[5]*CNISM, Dip. Fisica, Università di Camerino, Via Madonna delle Carceri, IT-62032 Camerino (MC), Italy*

[6]*Sincrotrone Trieste S.C.p.A., S. S. 14 km 163.5 Area Science Park IT-34149 Basovizza, Trieste, Italy*

(Received 18 November 2010; revised manuscript received 17 November 2011; published 5 January 2012)

The pressure behavior of an amorphous Si-rich SiGe alloy ($\alpha$-$Si_xGe_{1-x}$, $x = 0.75$) has been investigated up to about 30 GPa, by a combination of Raman spectroscopy, x-ray absorption spectroscopy, and x-ray diffraction measurements. The trends of microscopic structural properties and of the Raman-active phonon modes are presented in the whole pressure range. Nucleation of nanocrystalline alloy particles and metallization have been observed above 12 GPa, with a range of about 2 GPa of coexistence of amorphous and crystalline phases. Transformations from the amorphous tetrahedral, to the crystalline tetragonal ($\beta$-Sn) and to the simple hexagonal structures have been observed around 13.8 and 21.8 GPa. The recovered sample upon depressurization, below about 4 GPa, shows a local structure similar to the as-deposited one. Inhomogeneities of the amorphous texture at the nanometric scale, probed by high-resolution transmission electron microscopy, indicate that the recovered amorphous sample has a different ordering at this scale, and therefore the transformations can not be considered fully reversible. The role of disordered grain boundaries at high pressure and the possible presence of a high-density amorphous phase are discussed.

DOI: 10.1103/PhysRevB.85.045201 PACS number(s): 61.43.Dq, 64.70.kg, 78.30.Ly, 78.70.Ck

## I. INTRODUCTION

The study of amorphous semiconductors is of great relevance for both applied and theoretical physics. They are among the main constituents of electronic devices and photovoltaic cells and a deep understanding of their structure is essential. A detailed knowledge of their structure is also important for a complete interpretation of their physical and chemical properties, especially when structural modifications induced by the application of an external pressure occur. Disordered matter under extreme conditions of pressure and temperature can exhibit structural changes whose nature is not completely understood. An external pressurization can result in the atomic rearrangement into crystalline and nanocrystalline structures (pressure-induced crystallization[1–4]), thus opening the way to the study of new phases and metastable states. Compressed amorphous materials also show complex transformation during the pressure release, including the stabilization of new crystalline structures as well as the recovery of the initial amorphous one.[5–8] One of the most debated phenomena, postulated and sometimes observed in glassy and amorphous materials (especially those characterized by an open environment at ambient conditions), is the occurrence of "polyamorphism," that is the existence of different forms for the same amorphous material, usually characterized by different densities, atomic structures and/or physical properties (Refs. 9 and 10 and references therein).

Stimulated by previous results on $\alpha$-Si (Ref. 11 and references therein) and $\alpha$-Ge (Ref. 12 and references therein), showing the occurrence of dense disordered phases at high pressure, we have performed a detailed study of the pressure behavior of a Si-rich amorphous $Si_xGe_{1-x}$ alloy ($x = 0.75$) that can be considered a prototypical binary system for IV group semiconductors. Raman spectroscopy measurements were combined with x-ray techniques to provide a complete scenario of the transformations occurring in this system during compression up to 30 GPa and decompression down to ambient conditions. Solid-solid transitions associated with the metallization of the alloy have been detected and nanocrystalline phases have been grown upon pressurization. Reamorphization was observed during the unloading.

This manuscript is organized as follows: in Sec. II, a description of the sample preparation and its preliminary characterization will be given, together with details of the experimental techniques. A comprehensive discussion of the experimental results will follow in Sec. III. Concluding remarks will be given in Sec. IV.

## II. EXPERIMENTAL TECHNIQUES

The Si-rich amorphous SiGe alloy was prepared as film using a molecular beam epitaxy (MBE) apparatus, in order to control the stoichiometry during the growth. Evaporation was done over a common $SiO_2$ glass substrate at about 0.2 nm/s growth rate. An alloy with Si content of about 75% was prepared so to have a good balance among Raman signals associated with the Ge-Ge, Si-Ge, and Si-Si bond vibrations and a reasonable absorption jump for x-ray absorption spectroscopy (XAS) measurements at the Ge K-edge (transmission mode). The deposited amorphous film (about 300 nm thick) was obtained keeping the substrate temperature at about 80 °C and resulted in a powder once peeled off from the substrate.

All the preliminary characterizations and measurements described in this work were done on the sample after removal from the substrate of deposition. A needle was used to peel the sample off the substrate.

 

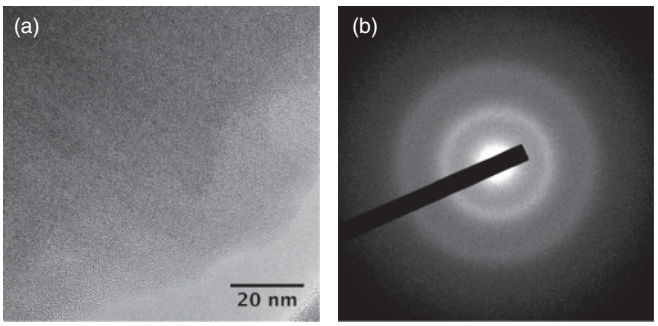


FIG. 1. High-resolution TEM image (a) and electron diffraction pattern (b) of as-deposited $\alpha$-SiGe (peeled off the substrate of deposition). The broad halo pattern is typical of amorphous materials.

A preliminary TEM analysis of the film was performed at IMPMC (Paris) using a JEOL 2100F microscope operating at 200 kV accelerating voltage, equipped with a field emission gun, a ultra-high-resolution (UHR) pole piece and a Gatan US4000 CCD camera. TEM analysis allowed to collect images of the sample down to about 0.2 nm resolution as well as electron diffraction (ED) patterns, reveling that the deposited film is homogeneous and amorphous (as shown by the high-resolution TEM image and the halo ED pattern typical of amorphous materials in Fig. 1). All the experiments at high pressure were performed using a 400 $\mu$m culets membrane diamond anvil cell (mDAC).[13,14]

Micro-Raman spectra as a function of pressure were collected using a T64000 spectrometer and an $Ar^+$ laser ($\lambda = 514.5$ nm) with spot size $\sim$2 $\mu$m. Laser power was about 100 mW onto the sample and a Mitutoyo $\times$20 objective was used. Two sets of measurements were collected in order to check the reproducibility of the observed transformations and the absence of spatial dishomogeneities. After removal from the substrate, a small amount of sample was loaded inside the gasket hole, on top of a thin NaCl layer as pressure transmitting medium.

Two sets of combined XAS and x-ray diffraction (XRD) measurements were collected up to about 30 GPa. Energy-dispersive XAS spectra were recorded at ODE (Optique Dispersive Exafs) beamline at Soleil Synchrotron, exploiting an upgraded setup for combined XAS/XRD acquisition.[15] X-ray absorption was measured in transmission mode at the Ge K-edge (11.103 keV) and the incident wavelength for diffraction was $\lambda = 1.118$ Å. Also, energy-scanning XAS measurements (Ge K-edge) were performed at the GSECARS (GeoSoilEnviroCARS) sector at Advanced Photon Source (APS), Argonne National Laboratory, taking advantage of a new setup available at 13-BMD Station, suitable for high-pressure measurements with diamond anvil cells.[16] Diffraction patterns were also collected using a MAR345 Image Plate detector and an incident wavelength of $\lambda = 0.62$ Å. Beam sizes were about $45 \times 45$ $\mu$m$^2$ and $15 \times 15$ $\mu$m$^2$ in the two beamlines, respectively. A stainless steel gasket was preindented to about 40 $\mu$m and a 150 $\mu$m hole was drilled and completely filled with sample, to ensure enough x-ray absorption at the Ge K-edge in the silicon-rich alloy. Different pressure transmitting media and pressure gauges were used in the two sets of measurements: silicone oil and a small ruby chip were loaded in the first case, while Ne and a small gold grain were used in the second one. Nonhydrostatic effects due to the use of NaCl as pressure transmitting medium can be neglected, as confirmed by the consistency of results obtained in different experiments where different media (including Ne) were used (see next section).

## III. RESULTS AND DISCUSSION

### A. Nucleation of crystalline phases by Raman scattering and XRD

Raman spectra at selected pressures are shown in Fig. 2. The three main bands characterizing the ambient pressure Raman pattern of the Si-Ge alloy (due to Ge-Ge, Si-Ge, and Si-Si optical stretching modes of vibration[17]) show a shift to higher frequencies up to 13.8 GPa, where a new weak band around 400 cm$^{-1}$ is observed. The corresponding peak positions versus pressure are reported in Fig. 3. Red crosses and blue stars (corresponding to two sets of measurements) are associated with the amorphous state, while magenta squares correspond to the Raman shift of the band observed above 13.8 GPa. Its Raman shift versus pressure is consistent with the TO vibrational mode of the Si-Si pair in the metallic $\beta$-Sn structure, whose Raman shift is also reported for

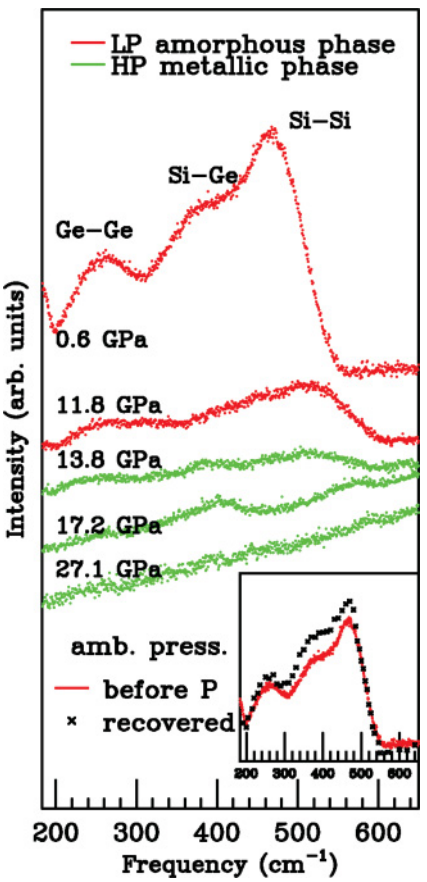


FIG. 2. (Color online) Raman patterns of the low-pressure amorphous state up to 11.8 GPa (red curves) and high-pressure phases (above 13.8 GPa, green curves). The inset shows ambient pressure spectra collected before (red line or light gray in the printed version) and after (black crosses) compression.

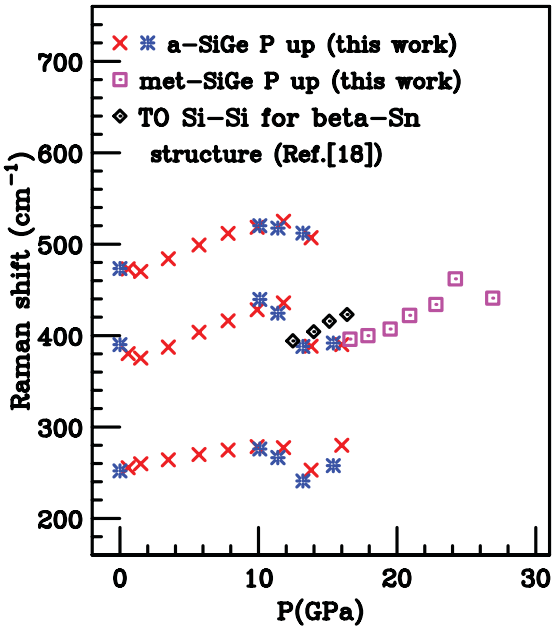


FIG. 3. (Color online) Raman shift vs pressure. The three modes of the amorphous alloy are indicated by red crosses and blue stars (two different sets of measurements). Magenta squares indicate the frequency of the high-pressure band. For comparison, also the Si-Si TO mode of the $\beta$-Sn structure of pure Si is reported (black diamond[18]).

comparison in Fig. 3 (black diamonds, from[18]). According to our Raman spectroscopy measurements, amorphous SiGe transforms to a crystalline phase consistent with the $\beta$-Sn structure starting from 13.8 GPa. Looking at Fig. 3, one can observe a softening of the Raman modes of the amorphous structure around 12 GPa, which can be interpreted as a transformation to a denser amorphous structure (HDA) just before the crystallization.

Diffraction patterns have been collected up to 29.0 GPa and a selection is reported in Fig. 4. Patterns up to 10.7 GPa (black solid curves) correspond to the amorphous phase, as can be observed by the broad band around $2\theta \sim 11^\circ$ corresponding to the first peak of the $S(q)$ for this system. The sharp Bragg peaks come from gold, used as pressure calibrant, tungsten (due to a possible contamination of the sample by the tungsten needle used for DAC loading), and the stainless steel gasket (indicated by the label "G"). Starting from 7.2 GPa, sharp peaks from Ne used as pressure transmitting medium are also visible.

In the pattern collected at 12.7 GPa (black dashed line), the broad band characteristic of the amorphous state is less intense and Bragg peaks associated with the crystalline tetragonal phase are observed, indicating the onset of crystallization. The coexistence of crystalline and amorphous grains at this pressure is not in contrast with the possible presence of higher-density amorphous domains. Unfortunately, a quantitative study of the amorphous component is not possible on the basis of this work.

The pressure value for the amorphous-to-crystalline transition obtained in the present study is in fair agreement with data available in literature.[19,20] In the crystalline phase, peaks

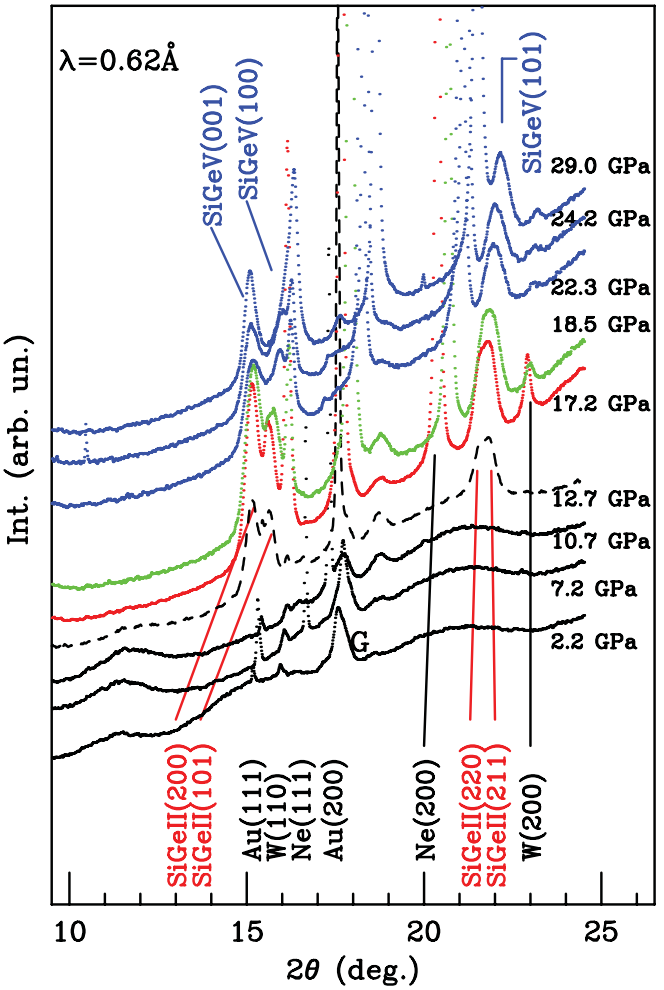


FIG. 4. (Color online) Diffraction patterns upon pressurization up to 29.0 GPa. The amorphous structure is observed up to 10.7 GPa (black patterns). Crystallization into the $\beta$-Sn phase starts at 12.7 GPa (dashed line) and goes on by further compression (red pattern at 17.2 GPa). Between 18.5 and 20.1 GPa patterns are compatible with both the simple hexagonal and the orthorhombic (*Imma*) structure (green). From 21.8 GPa, the simple hexagonal structure is obtained (blue). Spurious peaks from the gasket ("G"), gold, tungsten, and neon are also visible (see text).

from the alloy are the doublets around $2\theta \sim 15^\circ$ and $2\theta \sim 22^\circ$, which have been assigned to the (200), (101), (220), and (211) reflections of the $\beta$-Sn tetragonal structure (red curve), called SiGeII in analogy with the nomenclature used for pure Si and Ge.

Between 18.5 and 20.1 GPa, the structure is compatible with both the simple hexagonal (SH) and the orthorhombic (*Imma*) one (green curve). Starting from 21.8 GPa, the first Bragg peak shows a shift to lower angles as a function of increasing pressure and the second doublet transforms into a single peak. In this phase, the structure of the sample is consistent with SH [(001), (100) and (101) reflections, blue patterns]. In analogy with the nomenclature used for the hexagonal phase of pure Si,[21] we call this phase SiGeV.

The values of the lattice parameters obtained by fitting the diffraction patterns in the 17–30 GPa pressure range are reported in Fig. 5, lower panels. Red diamonds correspond to

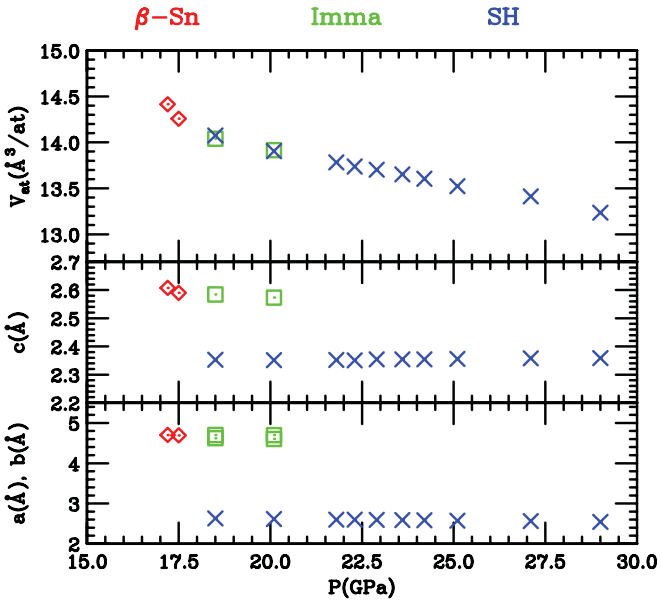


FIG. 5. (Color online) Lattice parameters and volume/atom of the unit cell of the crystalline phases obtained upon pressurization. Red diamonds are associated with the $\beta$-Sn structure, green squares with the orthorhombic *Imma*, and blue crosses with the simple hexagonal. The smooth decrease of the volume across the phase transitions suggests that they are continuous.

$\beta$-Sn, green squares refer to the *Imma* phase and blue crosses are used for the simple hexagonal.

In the upper panel, the volume/atom of the unit cell as a function of pressure is also reported. The continuous decrease of the volume upon compression (regardless the *Imma* structure is considered or not) suggests that the SiGe alloy undergoes a continuous $\beta$-Sn-to-SH phase transition.

Looking at the diffraction patterns associated with the crystalline phases of SiGe (patterns above 17.2 GPa in Fig. 4), one can also observe that the width of the Bragg peaks related to the alloy is always broader (typical full widths at half maximum are 0.2°) than that obtained for other substances contained in the sample environment (0.06° for Au used as the pressure marker, 0.04° for Ne, pressure transmitting medium). The peak width is related to the average size of the crystalline grains.[22] Standard approaches for the determination of crystallite sizes can be found in the literature and are based on the Scherrer's equation.[23,24] By application of these methods to our XRD patterns, we have estimated crystalline sizes of the order of 6(2) nm in the pressure range 17–30 GPa. This result is consistent with typical grain sizes deduced by inhomogeneities observed in the recovered sample, as will be further discussed in Sec. III C. The nanocrystalline nature of SiGe grown under pressure can play a role in the behavior of our sample under depressurization, as will be further discussed in the following.

### B. XAS analysis: edge shift and local structure

The amorphous-to-crystalline transition is accompanied by the metallization of the amorphous alloy. A shift of the Ge K-edge of about 0.5 eV toward lower energies has been observed by XAS measurements (in both energy-dispersive[15] and scanning-energy setups) around 13.9 GPa.

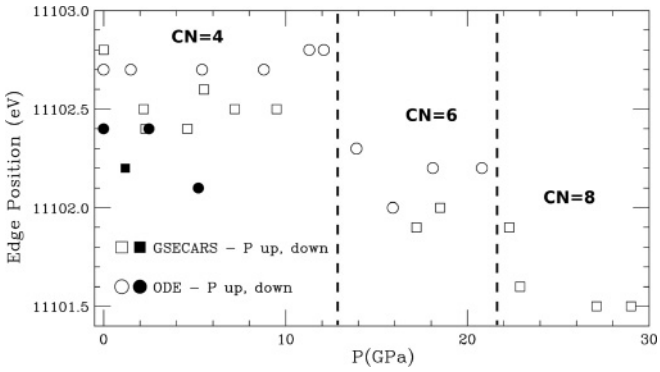


FIG. 6. Ge K-edge energy as a function of pressure obtained at GSECARS (squares) and at ODE (circles). Pressure makes the absorption onset occurring at a lower energy (open symbols). Once ambient conditions are recovered (filled symbols), the edge position is at a slightly lower energy as compared to its position before compression. The uncertainty in the edge position is ±0.3 eV.

In Fig. 6, the absorption edge position versus pressure obtained in both sets of XAS measurements (squares and circles correspond to GSECARS and ODE data, respectively) is reported. The transition from fourfold (amorphous) to sixfold ($\beta$-Sn) coordination and from sixfold to eightfold (simple hexagonal) coordination are associated with a shift of the edge toward lower energies of about 0.5 eV each (open symbols). This is simply interpreted as due to the closure of the semiconducting gap induced by the application of an external pressure,[25] resulting in a semiconductor-to-metal transition. The presence of a further energy shift associated with the six-to-eight fold coordination change can be qualitatively interpreted as due to an increased density of states in the conduction band, which slightly diminishes the energy of the last occupied state.

The analysis of the extended x-ray-absorption fine structure (EXAFS) region of the collected XAS spectra allowed the characterization of the local structure of our disordered alloy around the photoabsorber Ge atom. Using the GNXAS package[26,27] and a well established procedure (Ref. 28 and references therein), we reconstructed the structural EXAFS signal starting from the radial distribution function derived from molecular-dynamics (MD) calculations for $\alpha$-SiGe.[29,30] A simple first-shell model accounting for the first peak of the radial distribution was used to fit the experimental data. We considered only two-body first-neighbor signals [$\gamma^{(2)}$], due to the single scattering between the Ge-Ge and Si-Ge pairs, assuming a Gaussian bond-length distribution (upper green curves in Fig. 7). The EXAFS signals associated with the above mentioned MD simulations of the $\alpha$-SiGe structure at ambient conditions are compared with our experiment in Fig. 7 (lower curves), showing that a refinement of the relevant structural parameters (distance $R$ and variance $\sigma^2$) is necessary.

Our first shell best-fit model (green bottom curve) represents fairly well the experimental signal up to $k = 10$ Å$^{-1}$. At $k > 10$ Å$^{-1}$, the contribution from the Pt L3 absorption edge (from the Pt-coated focusing mirror at the GSECARS beamline) overlaps to the signal of our sample. First-neighbor

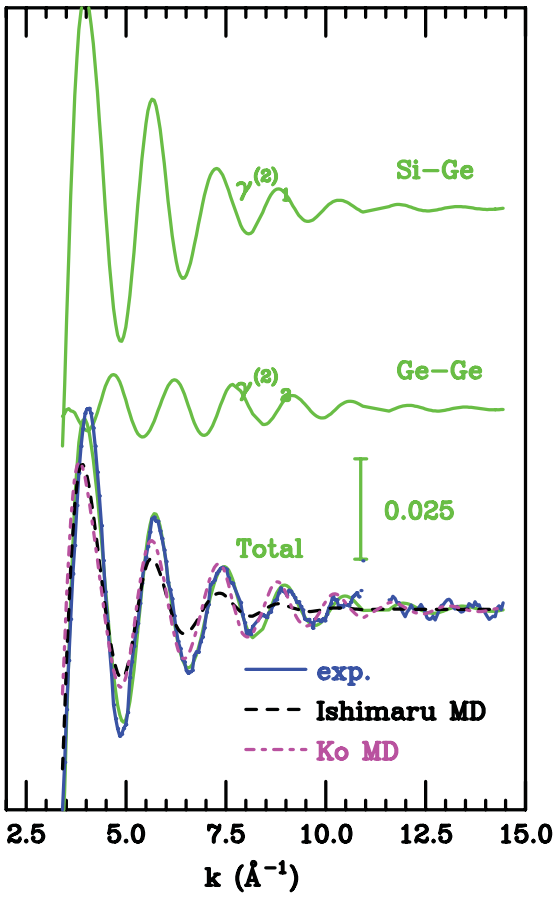


FIG. 7. (Color online) Fit of the reference XAS spectrum of $\alpha$-SiGe (blue continuous line), simulated adding single scattering signals [$\gamma^{(2)}$] due to the Si-Ge and Ge-Ge pairs (upper green curves). Comparison with results from MD simulations of Ko *et al.*[29] (magenta dot-dashed line) and Ishimaru *et al.*[30] (black dashed line) is also reported.

distances of $R_{\text{Ge-Ge}} = 2.44(1)$ Å and $R_{\text{Si-Ge}} = 2.40(1)$ Å were obtained at ambient conditions and the variance of the Si-Ge bond was $\sigma^2_{\text{Si-Ge}} = 0.0053(8)$ Å$^2$. These results are in good agreement with previous EXAFS results for $\alpha$-SiGe.[31–33]

In order to avoid the introduction of additional fitting parameters, some constrains were used in the fit of the high-pressure spectra. SiGe is known to form a randomly mixed alloy[17] (that is the probability of finding Ge or Si atoms as first neighbor is proportional to the atomic concentration), thus stoichiometry ($x = 0.75$) and coordination number (CN) were fixed. CN = 4,6,8 were used for the low-pressure amorphous, $\beta$-Sn (between 13.9 and 20.1 GPa) and SH structures (above 21.8 GPa), respectively.

Due to the limited amount of Ge contained in our alloy, the amplitude of the Ge-Ge signal is quite small ($N_{\text{Ge-Ge}} = \text{CN}/4$), thus for the high-pressure spectra, also $\sigma^2_{\text{Ge-Ge}}$ was fixed to the values obtained for pure amorphous Ge (0.0054 Å$^2$ at low pressure and 0.011 Å$^2$ above 10 GPa[7]).

Structural parameters as a function of pressure obtained by the fit of the experimental data are reported in Fig. 8 (squares and crosses are associated with ODE and GSECARS data, respectively). Green symbols have been used for the Ge-Ge pair and red ones for the Si-Ge pair. In the amorphous phase,

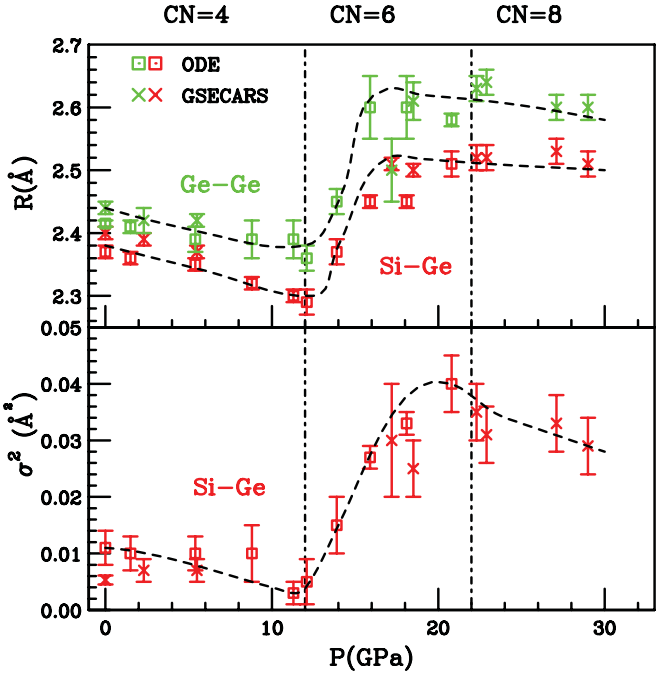


FIG. 8. (Color online) First-neighbor Ge-Ge and Si-Ge distances $R$ (upper panel) and Si-Ge bond variance $\sigma^2$ (lower panel) as resulted by the analysis of the EXAFS signals measured at GSECARS (crosses) and ODE (squares). Dashed lines are guides for the eyes.

the values of the first-neighbor distances (both $R_{\text{Ge-Ge}}$ and $R_{\text{Si-Ge}}$, upper panel) decrease under compression, reaching the values of 2.39(3) and 2.30(1) Å at 11.3 GPa. At 12.1 GPa, the onset of the transition to the $\beta$-Sn structure is observed by XRD measurements. Nevertheless, at this pressure, the signal is mainly dominated by the contribution of the amorphous structure, as can be seen by the corresponding values of the first-neighbor distances and their variances. By further increasing pressure, the values of the structural parameters start to increase. At 15.9 GPa, mean interatomic distances show an elongation of about 6% (Si-Ge) and 9% (Ge-Ge) as compared to the tetrahedral bonds and the typical bond-length distances above 22 GPa (hexagonal phase) are $R_{\text{Ge-Ge}} = 2.63(2)$ Å and $R_{\text{Si-Ge}} = 2.52(2)$ Å.

In the amorphous phase, the Si-Ge bond-length variance decreases down to $\sigma^2_{\text{Si-Ge}} = 0.003(2)$ Å$^2$ at 11.3 GPa and starts to increase in correspondence to the crystallization onset, as a consequence of the higher broadening of the first-neighbor distance distribution. The typical value of $\sigma^2_{\text{Si-Ge}}$ for the $\beta$-Sn structure is 0.027(2) Å$^2$ and the highest spread in the first-neighbor distances is obtained at 20.8 GPa, just before the transition to the SH structure.

### C. Reversibility of phase transitions

All the experimental techniques used in this study indicate that the pressure-induced crystallization of our alloy is a reversible transformation, since the amorphous structure is recovered upon pressure release from 29.0 GPa. Diffraction patterns collected upon decompression at ODE beamline (see Fig. 9) show that the high-pressure crystalline phase survives down to 5.2 GPa (green curves), then crystalline

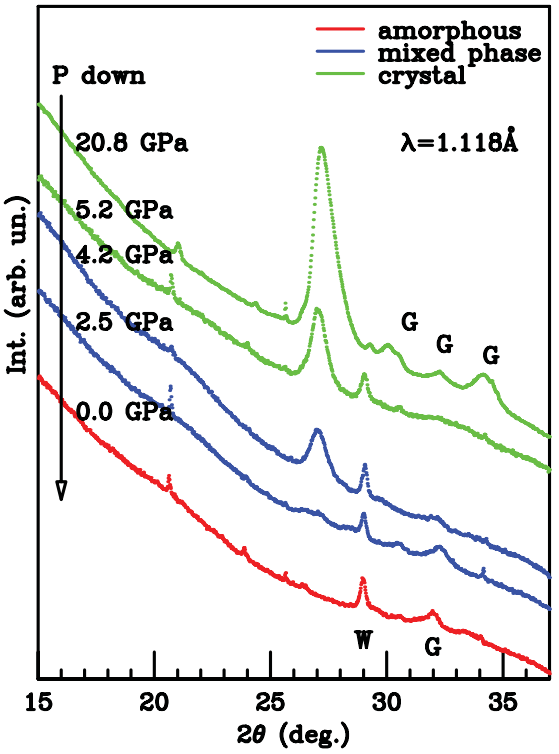


FIG. 9. (Color online) Diffraction patterns collected upon pressure download. The crystalline phase is observed down to 5.2 GPa (green patterns). At 4.2 GPa, the mixture of crystalline and amorphous structures is obtained (blue lines) and at ambient pressure, the amorphous state is recovered (red). Spurious peaks due to the gasket and tungsten needle contamination are also visible and indicated by the label "G" and "W", respectively.

and amorphous structures coexist between 4.2 and 2.5 GPa (blue curves) and an amorphous state is recovered at ambient pressure (red curve). The same phenomenon was observed during Raman spectroscopy (see inset of Fig. 2) and XAS measurements.

However, the analysis of the recovered sample by transmission electron microscopy (TEM) highlights some differences in the texture of the sample at the nanometric scale. In Fig. 10, a TEM image collected on the recovered sample is reported. If compared with the image collected on the initial (as-deposited) sample [see Fig. 1(a)], one can see that after compression the sample becomes inhomogeneous as clearly indicated by the textures visible in Fig. 10. The interpretation of this image is not trivial. It may suggest the presence of lower atomic density regions separating grains of amorphous SiGe of typical dimensions of the order of 5–10 nm. No traces of crystals (even at the nanometric scale) have been found on the recovered sample, as confirmed by TEM electron diffraction. Further investigation using high-angle annular dark field (HAADF) could help to clarify the possible variation of composition.

The occurrence of reversible phase transitions in amorphous SiGe has been proposed for Si-rich alloys.[20] Similar behaviors have been observed in other materials, like HDA-$H_2O$,[1] amorphous Ge,[7,34] porous amorphous Si[8] and multicomponent amorphous Zr-based alloy.[5]

A tentative explanation can be found considering the specific configurational Gibbs free-energy landscape $G(q,P,T)$

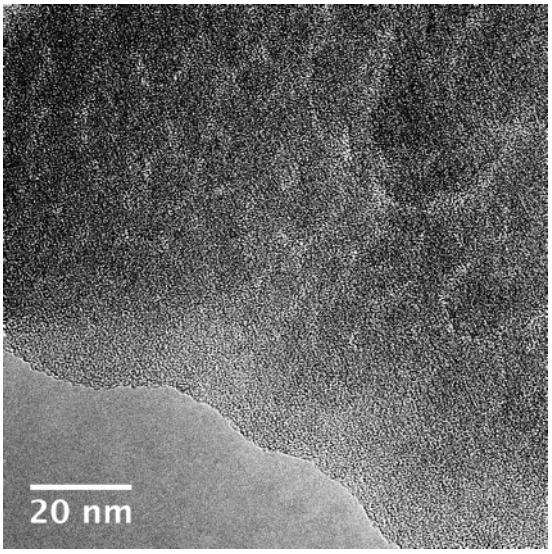


FIG. 10. TEM image of the recovered $\alpha$-SiGe. Inhomogeneities at the nanometric scale are present as a consequence of the pressurization/depressurization cycle.

(where $q$ is the ensemble of atomic configurations) explored by our systems during the pressurization cycles. In the configurational landscape, the stable phase is the one that minimizes the Gibbs free energy. Reaching that state requires enough thermal energy for overcoming the barrier between the absolute and local minimum reached by the actual system. In our experiment, XRD revealed that the high-pressure crystalline phase is an ensemble of nanocrystals of limited size (5–8 nm) separated by grain boundaries usually characterized by a high level of disorder (see Fig. 11 for a pictorial description, upper part). The Gibbs free energy of this system is likely to be higher than the absolute minimum associated with the stable phase, in the thermodynamic limit. Reaching this absolute minimum would require a heavy annealing process in such a way as to overcome the energy barrier separating these two minima. Our experiments have been performed at room temperature therefore the available thermal energy is only $E_t \sim k_B T \sim 26$ meV and as a matter of fact, is not enough to grow micrometric size crystals from the nanocrystalline ensemble. The available thermal energy and the energy barriers in the configurational landscape limit the phase space and the thermodynamic path explored by the system upon decompression, possibly assisting the recovery of the amorphous structure.

However, this structure is not exactly the same as the as-deposited one. In fact, although both are amorphous and show the same short-range atomic structure (according to Raman spectroscopy, XAS and XRD), the presence of inhomogeneities in the texture of the recovered sample at the nanometric level (bottom part of Fig. 11) reveals that a different polymorph for the same amorphous material is obtained upon decompression. As a whole, the recovered sample seems to be characterized by a higher degree of disorder, which is also consistent with the observation that the Ge K-edge position after the compression/decompression cycle is found at a lower energy (see Fig. 6 and Sec. III B).

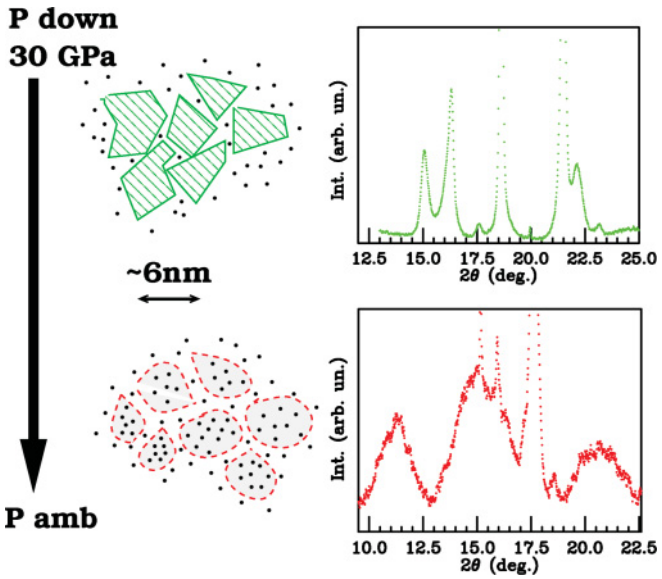


FIG. 11. (Color online) Schematic representation of the path followed by the SiGe alloy upon decompression. The high-pressure nanocrystalline $\beta$-Sn structure is represented by green dashed grains (∼6 nm), separated by disordered region associated with grain boundaries (dotted regions). In the recovered sample, the nanometric texture is retained (red-dashed lines) but grains are now characterized by an amorphous structure (lower panel). Typical diffraction patterns at 30 GPa and at ambient pressure are shown on the right (see caption of Fig. 4 for a detailed description of diffraction patterns).

## IV. CONCLUSION

In this work, the pressure-induced phase transitions undergone by a Si-rich alloy ($\alpha$-$Si_xGe_{1-x}$, $x = 0.75$) were studied in a wide pressure range (up to 30 GPa) upon compression and decompression by a combination of different and complementary experimental techniques (including Raman spectroscopy, XAS and XRD).

The extensive structural characterization revealed that before the complete crystallization into the tetragonal $\beta$-Sn phase (around 12 GPa), there is coexistence of amorphous and crystalline states, thus suggesting a possible existence of amorphous high-density domains. The metallization of the sample was observed at 13.8 GPa. At 21.8 GPa, a continuous phase transition to the simple hexagonal phase was observed, possibly through the intermediate orthorhombic *Imma* structure maybe observed between 18.5 and 20.1 GPa.

Upon depressurization from 29.0 GPa, the same sequence of phase transitions was obtained, as indicated by all the experimental techniques we used during this investigation. Starting from about 4 GPa, the sample transformed back to the semiconducting amorphous structure. The reamorphization process is quite continuous and traces of crystallinity were observed down to 2.5 GPa. The presence of nanocrystals in the recovered sample was excluded by the TEM analysis (imaging and electron diffraction).

This study has also highlighted a possible relation between the nanocrystalline nature of the high-pressure phase and the recovery of the amorphous structure once the sample comes back to ambient pressure. In particular, the disorder associated with grain boundaries characterizing the high-pressure structure could increase its Gibbs free energy, thus assisting the recovery of an LDA-like (low density amorphous) structure, rather than the stable zinc-blend one. The recovered amorphous polymorph was found to be characterized by a higher degree of disorder as compared to the as-deposited one.

The results obtained in this work stimulate further studies aimed to answer some open questions. For example, the occurrence of polyamorphism in this system deserves further studies. A careful characterization of the structure of the sample around 12 GPa on both nanocrystalline domains and amorphous textures would allow to confirm or exclude the presence of the HDA phase.

The phenomenon of reversibility of phase transitions deserves further theoretical and experimental investigation, aimed to clarify the mechanisms of reversible transformation and in which conditions and for which class of material it is likely to occur.

## ACKNOWLEDGMENTS

The authors acknowledge Soleil Synchrotron (France) and APS (Argonne, Illinois) for allocation of beamtime. Portions of this work were performed at GeoSoilEnviroCARS (Sector 13), Advanced Photon Source (APS), Argonne National Laboratory. GeoSoilEnviroCARS is supported by the National Science Foundation, Earth Sciences (EAR-0622171), and Department of Energy, Geosciences (DE-FG02-94ER14466). Use of the Advanced Photon Source was supported by the US Department of Energy, Office of Science, Office of Basic Energy Sciences, under Contract No. DE-AC02-06CH11357. Part of this work was performed under the auspices of US DOE by LLNL under contract number DEAC52-07NA27344.

*Now at: Lawrence Livermore National Laboratory, P.O. Box 808, Livermore, California 94551, USA; coppari1@llnl.gov

[1]R. J. Hemley, L. C. Chen, and H. K. Mao, Nature (London) **338**, 638 (1989).

[2]N. Hamaya, K. Sato, K. Usui-Watanabe, K. Fuchizaki, Y. Fujii, and Y. Ohishi, Phys. Rev. Lett. **79**, 4597 (1997).

[3]C. H. Polsky, L. M. Martinez, K. Leinenweber, M. A. VerHelst, C. A. Angell, and G. H. Wolf, Phys. Rev. B **61**, 5934 (2000).

[4]D. Machon, M. Daniel, V. Pischedda, S. Daniele, P. Bouvier, and S. LeFloch, Phys. Rev. B **82**, 140102 (2010).

[5]D. He, Q. Zhao, W. Wang, R. Che, J. Liu, L. X. J., and W. Wang, J. Non-Cryst. Solids **297**, 84 (2002).

[6]M. Xu, Y. Meng, Y. Q. Cheng, H. W. Sheng, X. D. Han, and E. Ma, J. Appl. Phys. **108**, 083519 (2010).

[7]F. Coppari, J. C. Chervin, A. Congeduti, M. Lazzeri, A. Polian, E. Principi, and A. Di Cicco, Phys. Rev. B **80**, 115213 (2009).

[8]N. Garg, K. K. Pandey, K. V. Shanavas, C. A. Betty, and S. M. Sharma, Phys. Rev. B **83**, 115202 (2011).
[9]P. H. Poole, T. Grande, C. A. Angell, and P. F. McMillan, Science **275**, 322 (1997).
[10]P. F. McMillan, J. Mater. Chem. **14**, 1506 (2004).
[11]D. Daisenberger, M. Wilson, P. F. McMillan, R. Quesada Cabrera, M. C. Wilding, and D. Machon, Phys. Rev. B **75**, 224118 (2007).
[12]O. I. Barkalov, V. G. Tissen, P. F. McMillan, M. Wilson, A. Sella, and M. V. Nefedova, Phys. Rev. B **82**, 020507 (2010).
[13]R. Letoullec, J. P. Pinceaux, and P. Loubeyre, High Press. Res. **1**, 77 (1988).
[14]J. C. Chervin, B. Canny, J. M. Besson, and P. Pruzan, Rev. Sci. Instrum. **66**, 2595 (1994).
[15]F. Coppari, A. Di Cicco, E. Principi, A. Trapananti, N. Pinto, A. Polian, S. Chagnot, and A. Congeduti, High Press. Res. **30**, 28 (2010).
[16]X. Hong, M. Newville, V. B. Prakapenka, M. L. Rivers, and S. R. Sutton, Rev. Sci. Instrum. **80**, 073908 (2009).
[17]N. J. Shevchik, J. S. Lannin, and J. Tejeda, Phys. Rev. B **7**, 3987 (1973).
[18]H. Olijnyk, Phys. Rev. Lett. **68**, 2232 (1992).
[19]A. Werner, J. Sanjurjo, and M. Cardona, Solid State Commun. **44**, 155 (1982).
[20]M. Imai, T. Mitamura, K. Yaoita, and K. Tsuji, in *Proceedings of the IV International Conference on High Pressure in Semiconductor Physics*, edited by D. S. Kyriakos and O. E. Valassiades (Aristotle University of Thessaloniki, Porto Carras, Greece, 1990).
[21]J. Z. Hu and I. L. Spain, Solid State Commun. **51**, 263 (1984).
[22]B. Warren, *X-Ray Diffraction* (Addison-Wesley, Reading, MA, 1969).
[23]J. I. Langford and A. J. C. Wilson, J. Appl. Crystallogr. **11**, 102 (1978).
[24]J. I. Langford, D. Louër, and P. Scardi, J. Appl. Crystallogr. **33**, 964 (2000).
[25]A. Filipponi, M. Borowski, P. W. Loeffen, S. De Panfilis, A. Di Cicco, F. Sperandini, M. Minicucci, and M. Giorgetti, J. Phys. Condens. Matter **10**, 235 (1998).
[26]A. Filipponi, A. Di Cicco, and C. R. Natoli, Phys. Rev. B **52**, 15122 (1995).
[27]A. Filipponi and A. Di Cicco, Phys. Rev. B **52**, 15135 (1995).
[28]A. Di Cicco, M. Minicucci, and A. Filipponi, Phys. Rev. Lett. **78**, 460 (1997).
[29]E. Ko, M. Jain, and J. R. Chelikowsky, J. Chem. Phys. **117**, 3476 (2002).
[30]M. Ishimaru, M. Yamaguchi, and Y. Hirotsu, Phys. Rev. B **68**, 235207 (2003).
[31]S. Minomura, K. Tsuji, T. Ishidate, K. Inoue, and M. Shibuya, J. Non-Cryst. Solids **59**, 541 (1983).
[32]L. Incoccia, S. Mobilio, M. G. Proietti, P. Fiorini, C. Giovannella, and F. Evangelisti, Phys. Rev. B **31**, 1028 (1985).
[33]M. Wakagi, T. Ohno, M. Chigasaki, and M. Nomura, J. Phys. Soc. Jpn. **56**, 2413 (1987).
[34]K. Tanaka, Phys. Rev. B **43**, 4302 (1991).